INTERNATIONAL JOURNAL FOR NUMERICAL METHODS IN FLUIDS
Int. J. Numer. Meth. Fluids 2006; **51**:469–487
Published online 20 December 2005 in Wiley InterScience (www.interscience.wiley.com). DOI: 10.1002/fld.1116

Numerical simulation of pollutant transport acted by wave for a shallow water sea bay

Sun Tao[1,*,†] and Tao JianHua[2,‡]

[1]*School of Environment, Beijing Normal University, Beijing 100875, People's Republic of China*
[2]*Department of Mechanics, Tianjin University, Tianjin 300072, People's Republic of China*

SUMMARY

A numerical model of pollutant transport acted by water waves on a shallow-water mild-slope beach is established in this study. The numerical model is combined with a wave propagation model, a multiple wave-breaking model, a wave-induced current model and a pollutant convection–dispersion model. The wave propagation model is based on the higher-order approximation of parabolic mild-slope equation which can be used to simulate the wave refraction, diffraction and breaking in a large area of near-shore zone combined with the wave-breaking model. The wave-induced current model is established using the concept of the radiation stress and considering the effect of bottom resistance caused by waves. The numerical model is verified by laboratory experiment results of regular and irregular waves over two mild beaches with different slopes. The numerical results agree well with experimental results.

The numerical model has been applied in the near-shore zone of Bohai bay in China. It is concluded that pollutant transport parallel to the shoreline due to the action of waves, which will induce serious pollution on the beach. Copyright © 2005 John Wiley & Sons, Ltd.

KEY WORDS: numerical model; water waves; pollutant transport; near-shore current; mild-slope beach

1. INTRODUCTION

Pollutant transport in the coastal zone is related closely to dynamic factors. Tide current had been taken as the main dynamic factor in studying pollutant transport in coastal zone for many years [1, 2]. With the development of the study on pollutant and sediment transport, the effect of wave-induced near-shore current for mild-slope beaches has gained attention gradually [3].

*Correspondence to: Sun Tao, School of Environment, Beijing Normal University, Beijing 100875, People's Republic of China.
†E-mail: suntao@bnu.edu.cn
‡E-mail: jhtao@tju.edu.cn

Contract/grant sponsor: State Key Project of Fundamental Research; contract/grant number: 2003CB415204
Contract/grant sponsor: National Natural Science Foundation of China (NSFC); contract/grant number: 59839330

Received 31 May 2004
Revised 12 September 2005
Accepted 14 September 2005

The vertical distribution of velocities may be influenced by wave propagation, especially in the area around wave breaking. Distribution of velocities will also be modified by the existence of the wave-induced current in near-shore zone, and the pollutant transport will be thus modified correspondingly. The effect of waves is significant for a mild-slope beach with shallow water, resulting in pollutant transport different from the results for a steep beach.

Rodriguez *et al.* [4] conducted an investigation on pollutant transport influenced by near-shore current induced by waves in coast. The effect of waves on pollutant transport was studied for an ideal plane sea bay [5]. The results indicated that the effect of waves is significant for the near-shore zone with mild slope. The pollutant transport can be simulated correctly only if the combined action of tide current and waves is considered.

A numerical model will be effective in studying the effect of waves in a large area of near-shore zone compared to an experimental model. A wave propagation model, a wave-induced current model and a pollutant convection–dispersion model should be included in the numerical model in order to simulate the pollutant transport caused by waves.

The basic requirement for the numerical model is the ability to simulate the wave propagation in a large area in studying the effect of waves on pollutant transport. There are two kinds of combined refraction–diffraction wave propagation models, which are Boussinesq model [6] and mild-slope equation [7]. The strong point in favour of the parabolic approximation of the mild-slope equation, proposed by Radder [8], is the speed of computation. The limitation of the parabolic model equation is the assumption of wave propagation within a limited range of angles about an assumed propagation direction in the earlier study. This limitation was relaxed by further research for increasing the range of allowed angles [9, 10]. Chawla *et al.* [11] simulated the evolution of wave spectra over a gently sloping bottom using the parabolic mild-slope equation and the model predicts dissipation due to wave breaking using a statistical breaking model.

When the waves propagate obliquely to the shoreline and break, the near-shore currents such as long-shore currents and rip-currents are generated. Longuet-Higgins [12] established the relationship between wave propagation and the resulting current using the concept of radiation stress, which is defined as the excess of momentum flux due to wave propagation.

The wave-induced near-shore current is usually considered to be the reason of sediment suspension in the near-shore zone. In this study, the distribution of wave-induced long-shore current and pollutant transport for a plane beach is studied based on numerical and experimental models. Validity of the numerical model is proved by the comparison with the results of the experimental model. The numerical model is also applied in the near-shore zone of Bohai Bay in China. The effect of waves on pollutant transport near the main outfall is studied based on the analysis of the distributions of velocities and the pollutant transport under the action of pure wave, and combined action of wave and tide.

2. MATHEMATICAL MODEL

2.1. Wave model

2.1.1. Regular wave model. The wave model is based on the higher-order approximate parabolic mild-slope equation given by Chawla *et al.* [11]. Choosing a coordinate system such that the x-axis is coincident to the incident wave propagation direction, the water surface

elevation is written as

$$\eta = \mathrm{Re}\{A(x, y)\mathrm{e}^{\mathrm{i}(\bar{k}x-\omega t)}\} \tag{1}$$

where $\mathrm{Re}(Z)$ denotes the real part of a complex number Z; $A(x, y)$ denotes the slowly varying complex wave amplitude; $\bar{k}$ is representative value of the wave number and defined as $\bar{k}(x) = \frac{1}{B}\int_0^B k(x, y)\,\mathrm{d}y$; ω is angular frequency; B is width of the domain; k is wave number.

The governing equation in the model for the complex wave amplitude is given as

$$\begin{aligned}
&(C_\mathrm{g}+U)A_x - 2\Delta_1 VA_y + \mathrm{i}(\bar{k}-a_0k)(C_\mathrm{g}+U)A + \left\{\frac{\sigma}{2}\left(\frac{C_\mathrm{g}+U}{\sigma}\right)_x - \Delta_1\sigma\left(\frac{V}{\sigma}\right)_y\right\}A \\
&+\mathrm{i}\Delta'\left[(p-V^2)\left(\frac{A}{\sigma}\right)_y\right]_y - \mathrm{i}\Delta_1\left\{\left[UV\left(\frac{A}{\sigma}\right)_y\right]_x + \left[UV\left(\frac{A}{\sigma}\right)_x\right]_y\right\} \\
&+\frac{\mathrm{i}\sigma k^2}{2}R|A|^2A + \frac{W}{2}A + \frac{-b_1}{k}\left\{\left[(p-V^2)\left(\frac{A}{\sigma}\right)_y\right]_{yx} + 2\mathrm{i}\left[\sigma V\left(\frac{A}{\sigma}\right)_y\right]_x\right\} \\
&+b_1\beta\left\{2\mathrm{i}\omega U\left(\frac{A}{\sigma}\right)_x + 2\mathrm{i}\sigma V\left(\frac{A}{\sigma}\right)_y - 2UV\left(\frac{A}{\sigma}\right)_{xy} + \left[(p-V^2)\left(\frac{A}{\sigma}\right)_y\right]_y\right\} \\
&-\frac{\mathrm{i}}{k}b_1\left[(\omega V)_y + 3(\omega U)_x\right]\left(\frac{A}{\sigma}\right)_x - \Delta_2\left\{\omega U\left(\frac{A}{\sigma}\right)_x + \frac{1}{2}\omega U_x\left(\frac{A}{\sigma}\right)\right\} \\
&+\mathrm{i}k\omega U(a_0-1)\left(\frac{A}{\sigma}\right) = 0
\end{aligned} \tag{2}$$

where $p = CC_\mathrm{g}$, C is phase velocity, i is imaginary unit, C_g is group velocity, U and V are currents in the x and y directions, respectively, and R is the factor of nonlinear influence.

$$R = \frac{\cosh 4kd + 8 - 2\tanh^2 kd}{8\sinh^4 kd} \tag{3}$$

where d is water depth. Also

$$\sigma = \omega - kU, \quad \beta = \frac{k_x}{k^2} + \frac{(k(p-U^2))_x}{2k^2(p-U^2)} \tag{4a}$$

$$\Delta_1 = a_1 - b_1, \quad \Delta_2 = 1 + 2a_1 - 2b_1, \quad \Delta' = a_1 - b_1\frac{\bar{k}}{k} \tag{4b}$$

The coefficients a_0, a_1 and b_1 could be chosen by a minimax approach in order to find the best approximation for wave propagation at large angles from the x direction [10]. W is the factor for energy dissipation.

The complex amplitudes for wave components at the offshore row is given as

$$A(0, y) = a\mathrm{e}^{\mathrm{i}k \sin\theta y} \tag{5}$$

where a is the wave amplitude for an offshore row, θ is the angle from the principal direction of wave propagation. Crank–Nicolson difference scheme is used to solve Equation (2) and the evaluation of all wave components as they travel towards shore can be computed simultaneously at each row.

2.1.2. Irregular wave model. Irregular wave fields are simulated using a spectral calculation method based on the discretization of the offshore wave spectrum $S(\omega, \theta)$, which indicates the distribution of wave energy over frequency and direction

$$S(\omega, \theta) = S(\omega)G(\omega, \theta) \tag{6}$$

where ω is angular frequency and θ is the angle from the principal direction of wave propagation. $S(\omega)$ is the frequency spectrum which indicates the distribution of wave energy over the frequency. The directional spreading function $G(\omega, \theta)$ indicates the distribution of wave energy over the direction.

Based on the offshore wave spectrum, the wave amplitude a_{jl} for an offshore row is written as

$$a_{jl} = \sqrt{2S(\omega, \theta)\Delta\omega\Delta\theta} \tag{7}$$

Indices j and l are used to represent frequency and direction, respectively. The water surface elevation can be represented by

$$\eta = \sum_j \sum_l \eta_{jl} = \mathrm{Re}\left\{ \sum_{j=1}^{N_f} \sum_{l=1}^{N_\theta} A_{jl}(x, y)\mathrm{e}^{\mathrm{i}(\bar{k}_j x - \omega_j t)} \right\} \tag{8}$$

N_f and N_θ are number of discretizations in frequency and direction, respectively, $k_j(x, y)$ is the wave number, ω_j is the angular frequency at the jth component.

$$A_{jl} = a_{jl}\mathrm{e}^{[\mathrm{i}(k_j \cos\theta_{jl} - \bar{k}_j)x + \mathrm{i}k_j \sin\theta_{jl} y]}$$

The transformation of each component is calculated by using the monochromatic mild-slope parabolic model. The statistical characteristics at the grid point are obtained by assembling the wave components by linear superposition. The significant wave height can be computed as

$$H_s(x, y) = \left(8 \sum_{j=1}^{N_f} \sum_{l=1}^{N_\theta} |A_{jl}(x, y)|^2 \right)^{1/2} \tag{9}$$

2.2. Multiple-wave-breaking model

The factor W in Equation (2) is related to energy dissipation. W is determined by the ratio of the dissipation rate δ_B to the wave energy E

$$W = \frac{\delta_B}{E} \tag{10}$$

where E, for small amplitude wave, is defined as $E = \frac{1}{8}\rho g H^2$, where H is wave height.

Dally *et al.* [13] assumed that the rate of loss of wave energy flux is dependent on the excess of energy flux over a stable value:

$$\delta_B = \frac{K_\mathrm{d}}{d}[EC_\mathrm{g} - E_\mathrm{s}C_\mathrm{g}]$$

K_d is dissipation coefficient, EC_g is local wave energy flow, $E_\mathrm{s}C_\mathrm{g}$ is stable wave energy flow, d is local water depth.

$$E_\mathrm{s} = \tfrac{1}{8}\,\rho g H_\mathrm{st}^2 = \tfrac{1}{8}\,\rho g(\Gamma d)^2$$

in which H_st is stable wave height, Γ is stable factor. Then the dissipation due to wave breaking could be written as

$$W = \frac{K_\mathrm{d}C_\mathrm{g}}{d}\left(1 - \frac{E_\mathrm{s}}{E}\right) = \frac{K_\mathrm{d}C_\mathrm{g}}{d}\left[1 - \left(\frac{\Gamma d}{H}\right)^2\right] \tag{11}$$

in general, $K_\mathrm{d} = 0.15$, $\Gamma = 0.4$. The model is suitable for simulating multiple-wave breaking.

Irregular wave breaking is more complex than that of regular waves. Setting an assumption similar to that of regular wave model and incorporating the fraction of breaking, Q_b, the average rate of energy dissipation in irregular wave breaking [14] can be expressed as

$$\overline{\delta_B} = \frac{K_1 Q_\mathrm{b} C_\mathrm{p}}{d}[E_\mathrm{m} - E_\mathrm{s}] \tag{12}$$

where

$$E_\mathrm{m} = \tfrac{1}{8}\,\rho g H_\mathrm{rms}^2$$

$$E_\mathrm{s} = \tfrac{1}{8}\,\rho g H_\mathrm{st}^2 = \tfrac{1}{8}\,\rho g(\Gamma_\mathrm{i} d)^2$$

K_1 is the proportional constant, C_p is the phase velocity related to the peak spectral wave period T_p, E_m is the local mean energy density, E_s is the stable energy density, H_rms is the root-mean-square wave height and Γ_i is the stable wave factor of irregular wave.

$$\bar{\delta}_B = \frac{K_1 Q_\mathrm{b} C_\mathrm{p} \rho g}{8d}[H_\mathrm{rms}^2 - (\Gamma_\mathrm{i} d)^2] \tag{13}$$

then

$$\bar{W} = \frac{\bar{\delta}_B}{E_\mathrm{m}} = \frac{K_1 Q_\mathrm{b} C_\mathrm{p}}{d}\left[1 - \left(\frac{\Gamma_\mathrm{i} d}{H_\mathrm{rms}}\right)^2\right] \tag{14}$$

The stable wave factor, Γ_i, is determined by

$$\Gamma_\mathrm{i} = \exp\left[K_2\left(-0.36 - 1.25\,\frac{d}{\sqrt{L_\mathrm{p} H_\mathrm{rms}}}\right)\right] \tag{15}$$

where L_p is the wavelength related to the peak spectral wave period, K_2 is the coefficient (0.1). Rattanapitikon and Shibayama [14] gave the explicit form of Q_b.

The breaking point is determined using the criterion proposed by Goda, which is written as

$$\left(\frac{H}{d}\right)_{\max} = \frac{\gamma\{1 - \exp[-1.5\pi d_b(1 + 15n^{4/3})/L_0]\}}{d_b/L_0} \tag{16}$$

where γ is a constant which is equal to 0.17 for regular wave and 0.15 for irregular wave [15]; L_0 is the deep-water wavelength, n is the bottom slope.

2.3. Wave-induced current model

The wave-induced current model is based on the concept of radiation stress, which indicates the excess of momentum flux due to wave propagation.

The depth-integrated equations of motion and water conservation can be written as

$$\left.\begin{aligned} \frac{\partial u}{\partial t} + \frac{\partial uu}{\partial x} + \frac{\partial vu}{\partial y} &= -g\frac{\partial \zeta}{\partial x} + T_x + M_x - B_x \\ \frac{\partial v}{\partial t} + \frac{\partial uv}{\partial x} + \frac{\partial vv}{\partial y} &= -g\frac{\partial \zeta}{\partial y} + T_y + M_y - B_y \end{aligned}\right\} \tag{17}$$

$$\frac{\partial \zeta}{\partial t} + \frac{\partial}{\partial x}[u(\zeta + d)] + \frac{\partial}{\partial y}[v(\zeta + d)] = 0 \tag{18}$$

where x and y are the horizontal coordinates normal and parallel to the shoreline, respectively; u and v are currents in the x and y directions, respectively; ζ is the mean surface elevation, T_x and T_y represent the forcing terms, with $D = \zeta + d$, there are

$$T_x = -\frac{1}{\rho D}\left(\frac{\partial}{\partial x}(S_{xx} + R_{xx}) + \frac{\partial}{\partial y}(S_{xy} + R_{xy})\right) \tag{19a}$$

$$T_y = -\frac{1}{\rho D}\left(\frac{\partial}{\partial x}(S_{xy} + R_{xy}) + \frac{\partial}{\partial y}(S_{yy} + R_{yy})\right) \tag{19b}$$

caused by the radiation stresses S_{ij} and R_{ij} due to rollers in breaking wave [16–18],

$$S_{xx} = E\left[\frac{C_g}{C}(1 + \cos^2\alpha) - \frac{1}{2}\right], \quad R_{xx} = 2E_r\cos^2\alpha \tag{20a}$$

$$S_{yy} = E\left[\frac{C_g}{C}(1 + \sin^2\alpha) - \frac{1}{2}\right], \quad R_{yy} = 2E_r\sin^2\alpha \tag{20b}$$

$$S_{xy} = S_{yx} = \frac{E}{2}\frac{C_g}{C}\sin 2\alpha, \quad R_{xx} = R_{yy} = E_r\sin 2\alpha \tag{20c}$$

where α is the wave angle, E_r is the roller energy per unit area:

$$E_r = 4\beta_r\frac{C}{gT}Q_b E \tag{21}$$

where $\beta_r \cong 0.9$. The cross-shore exchange of momentum is modelled as a dispersion term as follows:

$$M_x = \frac{\partial}{\partial x}\left(\varepsilon \frac{\partial u}{\partial x}\right) + \frac{\partial}{\partial y}\left(\varepsilon \frac{\partial u}{\partial y}\right) \tag{22a}$$

$$M_y = \frac{\partial}{\partial x}\left(\varepsilon \frac{\partial v}{\partial x}\right) + \frac{\partial}{\partial y}\left(\varepsilon \frac{\partial v}{\partial y}\right) \tag{22b}$$

where ε is dispersion or mixing coefficient,

$$\varepsilon = \varepsilon_{bw} + \varepsilon_{bf} + \varepsilon_{br} = C_1 \frac{H^2 g T}{4\pi^2 d} \cos^2 \alpha + C_2 u_m H + C_3 (d + \zeta)\left(\frac{D_b}{\rho}\right)^{1/3} \tag{23}$$

ε_{bw} is related to wave action, ε_{br} is related to wave breaking, and ε_{bf} is related to bottom fiction dissipation. Parameters C_1, C_2, C_3 could be settled as $0.5, 0.1$ and 0.025, respectively [19], and then the influence of wave propagation, wave breaking and bottom friction could be included in cross-shore exchange of momentum.

Bottom stress on the combined action of wave and current is calculated as

$$B_x = \frac{\rho g u\sqrt{u^2+v^2}}{C^2} + \frac{\pi\rho}{8} f_w \sqrt{u_w^2 + v_w^2}\, u_w + \frac{F_B \rho}{\pi}\sqrt{2}\left(\frac{g}{C^2} f_w\right)^{1/2} \sqrt{u^2+v^2}\, u_w \tag{24a}$$

$$B_y = \frac{\rho g v\sqrt{u^2+v^2}}{C^2} + \frac{\pi\rho}{8} f_w \sqrt{u_w^2 + v_w^2}\, v_w + \frac{F_B \rho}{\pi}\sqrt{2}\left(\frac{g}{C^2} f_w\right)^{1/2} \sqrt{u^2+v^2}\, v_w \tag{24b}$$

where u_w, v_w are particle velocities at bottom in the x and y directions, respectively. F_B is factor of wave–current interaction influence, which is 0.917 when the directions of wave and tide are parallel, -0.1983 for the directions of wave and tide are vertical and 0.352 for other conditions. f_w is wave bottom friction factor.

The finite difference scheme is used for calculating the equation. At the beginning of the calculation, the initial velocities are set to zero,

$$\zeta = 0, \quad u = 0, \quad v = 0 \tag{25}$$

All velocities parallel to the boundary are set to zero in the calculation for the closed boundary. The velocities outside the boundary are set to the same value as the corresponding velocity inside the domain, but obtain a negative sign.

$$v_i = 0, \quad u_i = -u_{i+1} \tag{26}$$

A free slip boundary condition is used by assuming zero gradient of a variable perpendicular to the open boundary,

$$\frac{\partial u}{\partial n} = 0, \quad \frac{\partial v}{\partial n} = 0 \tag{27}$$

A space-staggered grid system is used, with the water depth being located at the grid centre, with u and v at the centre of the grid sides and the water elevation at the node of the grid. The scheme is basically second-order accurate both in time and space with no stability constraints due to the time centred implicit character of the ADI technique. With the initial and boundary conditions included, the resulting finite difference equations for each half time step are solved using the method of Gauss elimination and back substitution.

2.4. Pollutant convection–diffusion model

The two-dimensional convection–diffusion equation integrated along depth is written as

$$\frac{\partial(DS)}{\partial t} + \frac{\partial(DuS)}{\partial x} + \frac{\partial(DvS)}{\partial y} = \frac{\partial}{\partial x}\left(K_{xx}D\frac{\partial S}{\partial x}\right) + \frac{\partial}{\partial x}\left(K_{xy}D\frac{\partial S}{\partial y}\right) + \frac{\partial}{\partial y}\left(K_{yx}D\frac{\partial S}{\partial x}\right) + \frac{\partial}{\partial y}\left(K_{yy}D\frac{\partial S}{\partial y}\right) + DS_{\mathrm{m}} \tag{28}$$

where $D = \zeta + d$ is total water depth, S is concentration, u and v are velocities along x, y directions, respectively, S_{m} is source term, K_{ij} is depth average dispersion–diffusion coefficient (m^2/s), which are calculated as

$$K_{xx} = \frac{(\alpha u^2 + \beta v^2)D\sqrt{g}}{C\sqrt{u^2+v^2}} \tag{29a}$$

$$K_{xy} = K_{yx} = \frac{(\alpha - \beta)uvD\sqrt{g}}{C\sqrt{u^2+v^2}} \tag{29b}$$

$$K_{yy} = \frac{(\alpha v^2 + \beta u^2)D\sqrt{g}}{C\sqrt{u^2+v^2}} \tag{29c}$$

where α, β are the depth-averaged longitudinal dispersion and lateral turbulent diffusion coefficients, respectively, which are settled as 5.93 and 0.23 [20].

The finite difference scheme used in this model is based on the ADI and modified by Chen and Falconer [25], which involves the sub-division of each time step into two half-time steps. In the first half-time step, the water elevation, u and the solute concentration are implicitly in the x direction. Similarly, for the second half-time step, the water elevation, v and the solute concentration are implicitly in the y direction. The upwind scheme is applied to convection to reduce the effect of numerical viscosity.

The closed boundary condition for the solute is

$$\frac{\partial S}{\partial n} = 0 \quad \text{and} \quad \frac{\partial^2 S}{\partial n^2} = 0 \tag{30}$$

which means that the concentration does change parallel to the close boundary and there is no solute flux across the solid boundary. n is the direction perpendicular to the closed boundary. As for the open boundary, there is

$$S = S_0 \tag{31}$$

which describe the condition that the boundary values S_0 are known. The methods of interpolation used for the case of S_0 are unknown.

The third-order accuracy difference for the convection term and second-order accuracy difference for diffusion term are used to solve Equation (28).

In order to validate the numerical model, the models results are first compared with analytical solutions.

Equation (32) indicates an analytical solution for solving the two-dimensional convection–diffusion equation in a rectangular region the concentration $C(x, y, t)$ at a given time t for a point source pollutant placed at the centre of the domain (x_0, y_0) [22]

$$C(x, y, t) = \frac{K}{\sqrt{4\pi K_x t}\sqrt{4\pi K_y t}} \exp\left[-\frac{(x - x_0 - Ut)^2}{4K_x t} - \frac{(y - y_0 - Vt)^2}{4K_y t}\right] \tag{32}$$

where (x_0, y_0) is the location of the point source, K is a scaling factor, which is taken to be 1.0×10^{12} for the test case. t is the time for pollution transport, U and V are the velocities in the x and y directions, respectively, K_x, K_y are the diffusion coefficient in the x and y directions. Uniform horizontal velocities of $U = V = 0.5\,\text{m/s}$, $K_x = K_y = 1 \times 10^4\,\text{m}^2/\text{s}$, time step $\Delta t = 50\,\text{s}$ and grid spacing $\Delta x = \Delta y = 5000\,\text{m}$ are used in the calculation.

Figure 1 gives the comparison between numerical and analytical solution in the section of direction after $t = 36000\,\text{s}$ and $72\,000\,\text{s}$. The agreement with each other is quite good.

Wave propagation model, wave-breaking model, wave-induced current model and pollutant convection–diffusion model constitute the numerical model for the study of the effect of waves on pollutant transport in the near-shore zone.

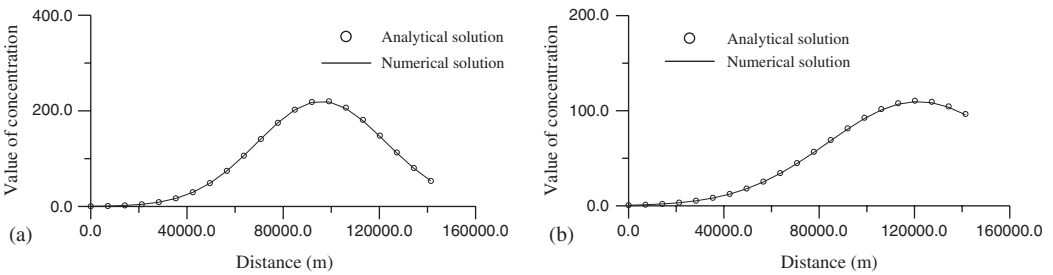

Figure 1. Concentration distribution for convection and diffusion by analytical and numerical solutions after: (a) 36 000 s; and (b) 72 000 s.

3. NUMERICAL MODEL TEST

In order to validate the numerical model, the distribution of long-shore current and pollutant transport acted by the regular and irregular waves with different wave factors are investigated over two mild beaches with different slopes by physical experiment and numerical simulation.

The experiment is performed in a wave basin, 42.6 m long, 24.0 m wide and 1.0 m deep. The plane beach was rotated at 30° with respect to the wave maker in order to increase the length of the beach and to make the wave propagate obliquely to the shoreline (Figure 2). The beach slopes of $\frac{1}{100}$ and $\frac{1}{40}$ are adopted. For the $\frac{1}{100}$ beach, the constant depth before the slope is 0.18 m, while for $\frac{1}{40}$ beach it is 0.45 m.

The wave heights are measured with 40 capacitance wave gauges placed in three lines normal to the shoreline. The long-shore current velocities are measured with flow metres located in two lines normal to the shoreline, and one-third of the water depth from the bottom, which is near the position of the depth-averaged long-shore current velocity. Each line has 16 flow metres.

The plane beach in the experiment has been painted white and the grid-lines (1 m × 1 m) were drawn on the surface of the beach. Pollutant transport is recorded by tracking the released dye using a video camera placed at 8 m above the sea surface.

3.1. *Wave-induced long-shore current*

The results shown in Figure 3 are the numerical results of wave-induced long-shore currents on the plane beach.

Figure 4 gives the comparison between numerical and experimental results of the cross-shore distribution of long-shore current velocities under the action of regular and irregular waves. The x-coordinate denotes the distance seaward from the coastline. The solid lines correspond to the results calculated by wave-induced current model, and the circles correspond to experimental results. The discrepancies between the observed and model-predicted results, especially at the position before wave breaking, are influenced by the parameters of dispersion coefficient in Equation (22). The spectral sea state was obtained by using Wen spectrum in the calculation of irregular wave propagation, while the Wen spectrum was proposed based on the field data in the near-shore zone of China [24].

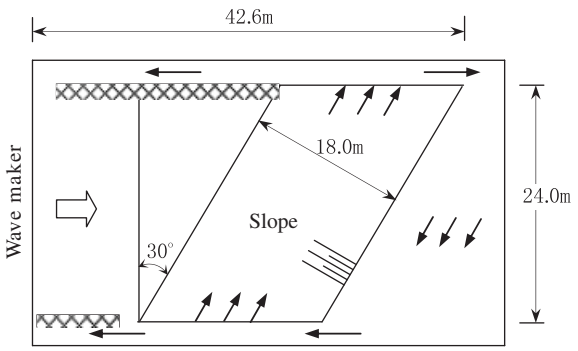

Figure 2. Experimental set-up [23].

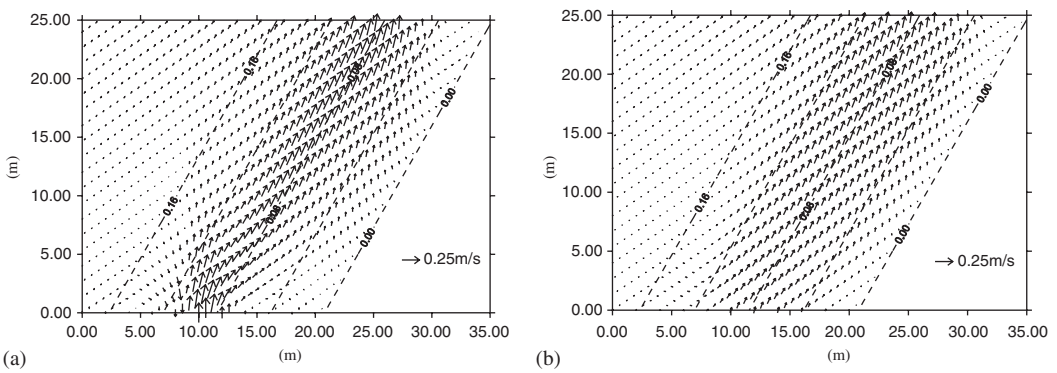

Figure 3. Numerical results of wave-induced long-shore currents in the plane beach, beach slope 1/100: (a) acted by regular waves, incident wave period $T = 1.0$s; incident wave height $H = 0.07$ m; and (b) acted by irregular waves, incident average wave period $T = 1.0$ s; incident average wave height $H = 0.05$ m.

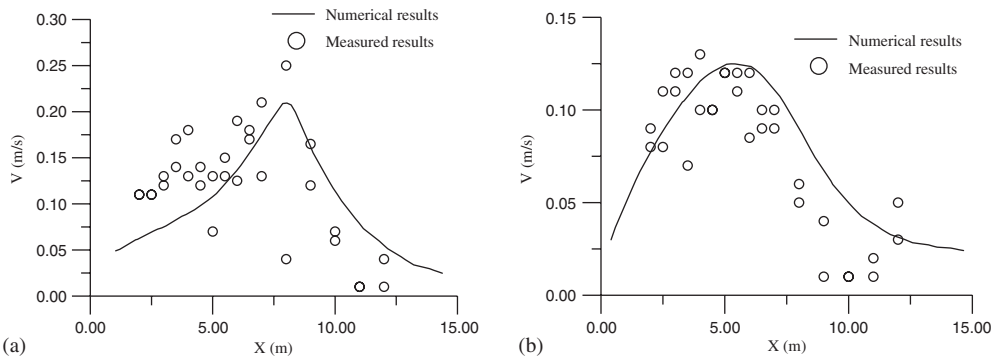

Figure 4. Cross-shore distribution wave-induced long-shore currents, beach slope 1:100: (a) acted by regular waves, incident wave period $T = 1.0$ s; incident wave height $H = 0.07$ m; and (b) acted by irregular waves, incident average wave period $T = 1.0$ s; incident average wave height $H = 0.05$ m.

The distribution of long-shore current is dominated by wave breaking. Velocity is small before wave breaking and it is increased when the wave heights are reduced abruptly near the wave-breaking area. The peak value of current velocity is located inside of the surf-zone.

For irregular waves, the highest waves tend to break at the greatest distances from the shoreline. There is no clear breaking point compared to regular waves. The area of energy dissipation for irregular wave breaking is greater than that of regular waves. Cross-shore distributions of current induced by multi-directional irregular waves are more gentle.

Figure 5 gives the cross-shore distributions of long-shore current induced by regular and irregular waves with different incident wave heights.

With the increase in incident wave height, the maximum velocity of long-shore current and its distance offshore will be increased accordingly. The effect of wave-induced currents should be considered especially for the waves with higher incident wave height.

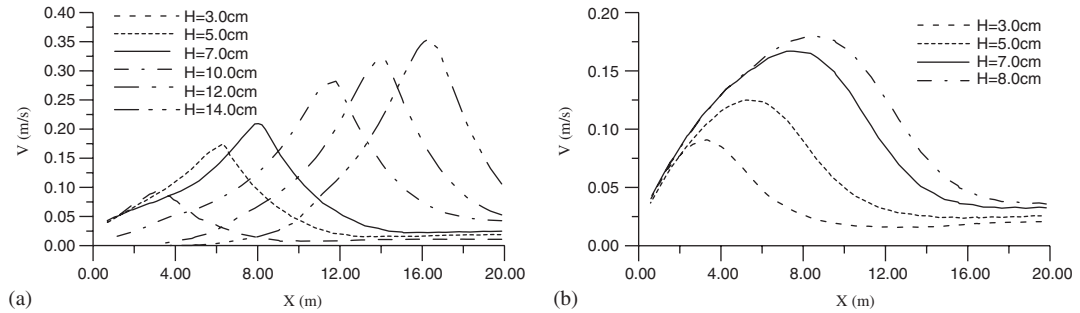

Figure 5. Cross-shore distribution long-shore currents on the action of regular (a) and irregular waves (b) with different incident wave heights. Beach slope 1:100: (a) incident wave period $T = 1.0$ s; and (b) incident average wave period $T = 1.0$ s.

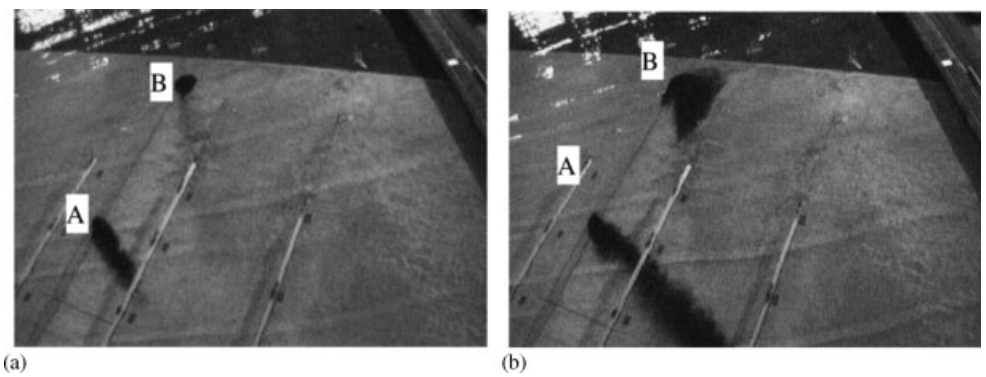

Figure 6. Processes of dye transport under the action of waves after different times of discharge. Points A and B indicate the positions of outfalls located inside and outside of the surf-zone.

3.2. The effect of wave on pollutant transport

The image shown in Figure 6 recorded the process of dye transport discharged from different positions on the action wave for the plane beach (shown as Figure 2).

Images (a) and (b) in Figure 6 denote the results of dye transport after different times of discharge. Points A and B indicate the positions of outfalls located inside and outside of the surf-zone. The dye discharge from these two positions is simultaneous in the experiment. It is concluded that the dye discharge inside the surf-zone will transport parallel approximately to the shoreline under the action of waves. While the dye transport outside the surf-zone is hardly affected by wave action.

Figure 7 indicates numerical results of pollutant concentration acted by regular waves, which are discharged at the different positions. The distances of discharge outfalls from the shoreline are different in the calculation. Results for different beaches with different slopes are compared in Figures 7(a) and (b).

Points A, B, C and D indicate the position of the outfall. With incident wave height $H = 0.07$ m and incident wave period $T = 1.0$ s, points A, B, C are located in the surf-zone

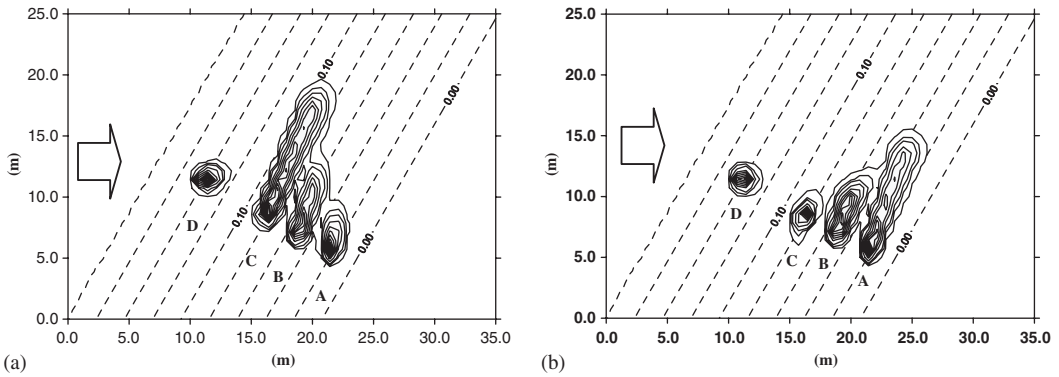

Figure 7. Contours of pollutant concentration acted by regular waves, which are discharged at the different distances from the shoreline, incident wave height $H = 0.07$ m; incident wave period $T = 1.0$ s. After 70.0 s of released: (a) beach slope 1:100; and (b) beach slope 1:40.

where pollutant transport is parallel to the shoreline in the beach with slope of $1/100$. There is hardly any influence of waves on the pollutant discharge outside of the surf-zone (D). Because of the difference in wave breaking, the effect of waves on pollutant transport is greater for the mild-slope beach than for the beach with $\frac{1}{40}$ slope.

Numerical and experimental results prove that the pollutant transport in the area outside of the surf-zone is not significantly affected by waves, while pollutant transport will be approximately parallel to the shoreline under the action of waves in the surf-zone, which causes contamination of spread even far away from the discharge outfall. Therefore, it is necessary to consider the effect of waves in analysing the environment of a mild-slope beach with shallow water.

3.3. Wave-induced current in the near-shore zone

Based on the comparison with experimental and numerical results, it is proved that the numerical model is suitable to simulate the pollutant transport under the action of waves for the near-shore zone. Before the application on a natural near-shore zone, the wave-induced current model is applied in an ideal topography, which is written as

$$x_c = 400 \cos^2[\pi(y - 400)/2000] \tag{33a}$$

$$h = 20(2000 - x_c - x)/(2000 - x_c) \tag{33b}$$

where h is water depth; x and y indicate the cross and long-shore directions, respectively. Figure 8(a) gives the topography. Wave propagation to the shoreline is along the x direction.

When the waves approach the shoreline and break, radiation stresses will be induced with dispersion of wave energy towards the shoreline. As for waves propagating obliquely to the shoreline, the gradient of radiation stresses along the shoreline will be balanced by bottom stress and then the long-shore current is induced.

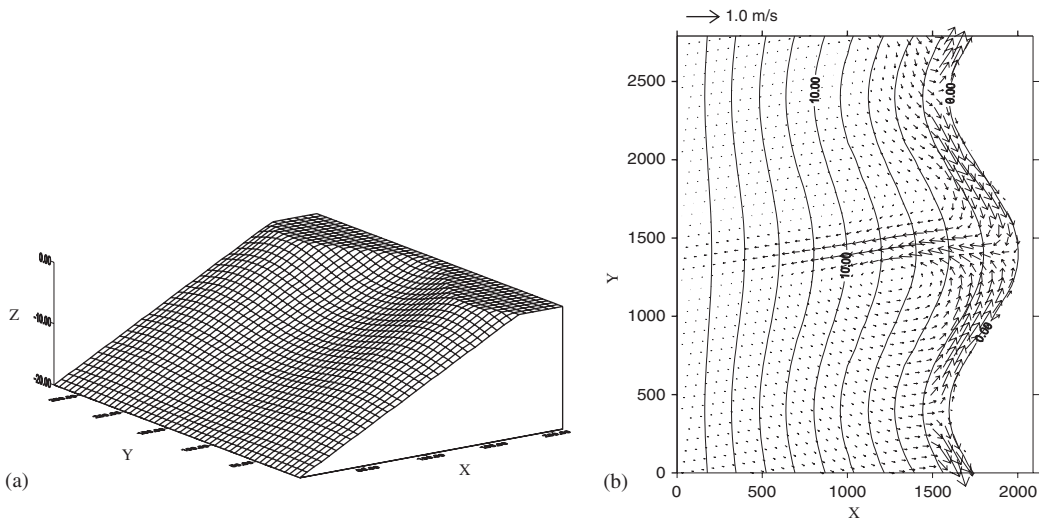

Figure 8. Wave-induced near-shore currents in an ideal topography: (a) topography; and (b) near-shore current.

Figure 8(b) gives the wave-induced near-shore current in the topography decided by Equation (33). The direction of wave-induced near-shore current is from the convex to the concave area. Rip-current occurs in the concave area satisfying mass balance equation. The influence range of rip-current will not be confined to the surf-zone, but persists outside of the surf-zone even without the forcing terms. Similar reasoning could also be applied to analysing the shoreward current, which occurs in the convex area.

The results indicate that the long-shore current is weak outside of the surf-zone and concentrated in the intense area of wave breaking. The velocity is small near the shoreline. Distribution of near-shore currents is changed greatly with the variation of direction of incident waves.

4. APPLICATION OF NUMERICAL MODEL IN A SHALLOW WATER SEA BAY

The coastal region around Bohai sea (People's Republic of China) is the economy centre in north of China and will become the emphasis of economy development in the new century. Bohai bay is a typical mild-slope beach with shallow water. With the high-speed development of economy near the coastal region, the water quality has been seriously deteriorated due to the wastewater from Beijing, Tianjin and Hebei province and the ecological environment has been exacerbated and red tides appear frequently.

The pollutant transport on the action of wave from directions of east (E) are studied specially in paper. Topography used in calculation is shown as Figure 9.

The numerical model is also applied to the pollutant transport under the action of wave in Bohai bay, which is a typical mild-slope beach with shallow water in the west of Bohai sea in China. The pollutant transport in the near-shore zone of Bohai bay under the action of

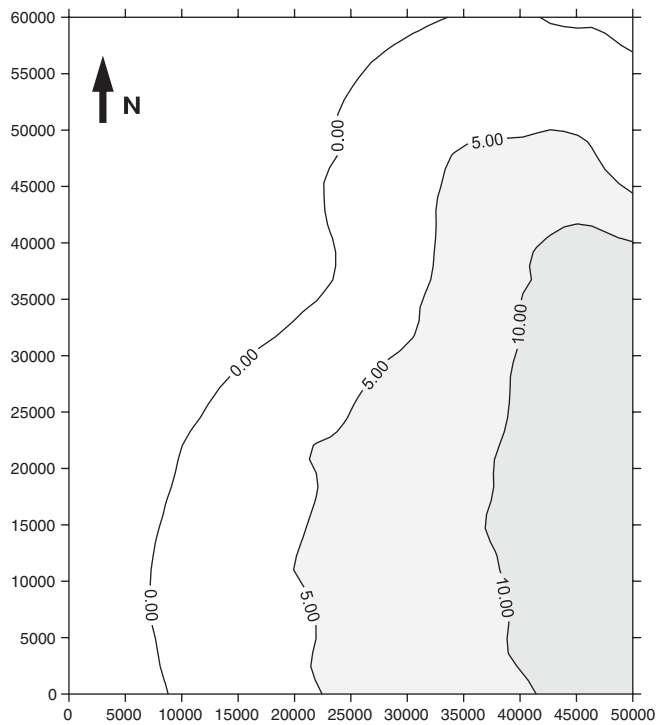

Figure 9. Topography for calculation (m).

waves from the directions of east (E) and east–south–east (ESE) are simulated specifically in this study.

The wave field is calculated by the parabolic mild-slope equation, and then radiation stress is obtained. The space step length of the calculation is $\Delta x = \Delta y = 10.0$ m.

The flooding and drying processes used are presented by Lin and Falconer [25]. 'Wet' and 'dry' cells are settled to represent the model area as potentially wet cells and land cell cells. At the end of every half-time step, the depth at the each grid cell side is scanned. If all four side depths for any grid cell or the average centre depth are less than a pre-determined value $L1$ (the bed roughness was used in the study), the grid cell is assumed to be dry the cell is removed from the computational domain.

If any side depth becomes less than $L1$, both the corresponding depth and the velocity are set at zero. If the average depth of a wet cell is larger than $L1$, but less than $L2$ (2.0 $L1$), the grid cell is considered potentially dry, and the grid cell should be removed from the computational domain for the flow direction from the potentially dry cell is towards the adjacent wet cell.

The near-shore currents induced by the waves from the direction of E and ESE are shown in Figure 10; the incident wave height is 2.9 m and 3.31 m, respectively, and wave period is 7.6 s.

Wave-induced currents and tide current usually exist simultaneously in the near-shore zone. The results shown in Figures 11(a) and (b) represent the distributions of

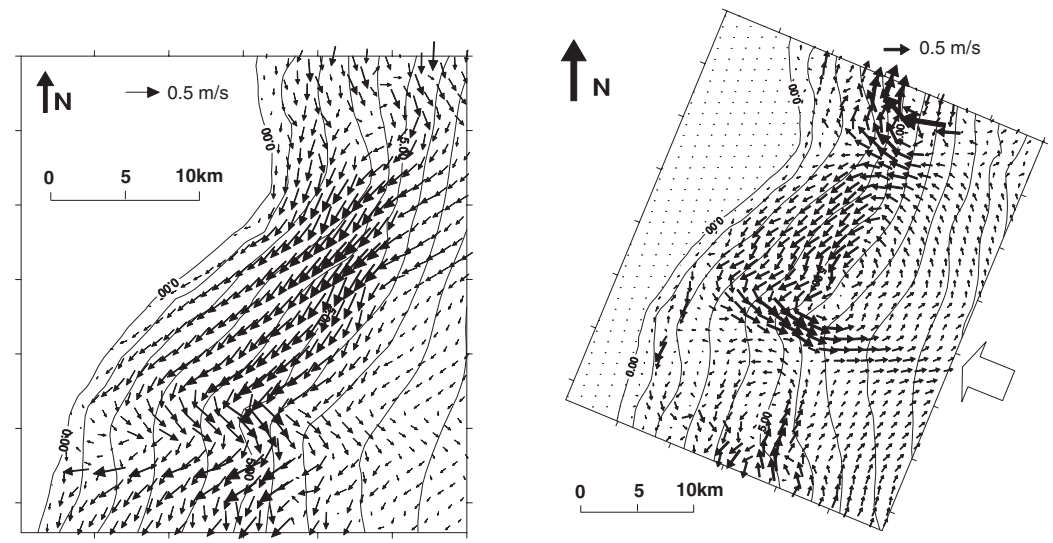

(a) (b)

Figure 10. Wave-induced near-shore currents in the near-shore zone of Bohai Bay: (a) from the direction of E, incident wave period $T = 7.6$ s, incident wave height $H = 2.9$ m; and (b) from the direction of ESE, incident wave period $T = 7.6$ s, incident wave height $H = 3.31$ m.

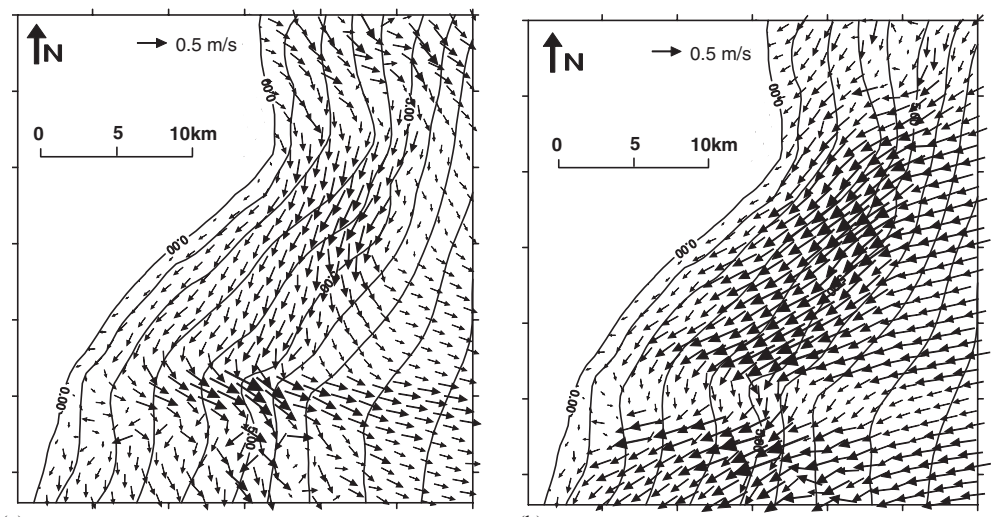

(a) (b)

Figure 11. Distribution of currents under the combined action of waves and tide currents, incident wave height is 2.9 m, period is 7.6 s: (a) Ebb tide; and (b) flood tide.

velocities under the combined action of tide currents and waves. Wave-induced current has the same order of magnitude as the tide current in the near-shore zone of mild-slope beach.

Effects of waves on pollutant transport in the near-shore zone of Bohai bay are studied by comparing the pollutant transport discharging from different outfall positions under pure wave and combined wave and tide action. Pollutant transport is expressed using the concept of contaminated probability, which is defined as the percentage of cumulative time contaminated to the total time of the study, it is calculated as

$$P(x_i, y_i) = \sum_{i=1}^{N} k_j \frac{\Delta t}{T_0} \tag{34}$$

where Δt is the time space, T_0 is the time of the study, $N = T_0/\Delta t$. The parameter k_j equal to 1 when the concentration exceeds a certain value, otherwise $k_j = 0$.

Figure 12 shows the contour of contaminated probability under the action of pure waves (Figure 12(a)), combined action of waves and tide (Figure 12(b)) for different outfall positions $(\cdots)$ after disposal in 24.0 h.

The pollutant transport is influenced significantly by the action of waves at certain areas. The contaminated area under the combined action of waves and tide is similar to the result under the action of pure waves. The near-shore zone will be contaminated under the action of waves even far away from the outfall. The effect of tide current extends the contaminated area in the cross-shore direction.

The study on the pollutant transport acted by waves in a mild-slope beach with shallow water is beneficial to the understanding of the contamination of the near-shore zone and to the engineering of ocean disposal of waste water.

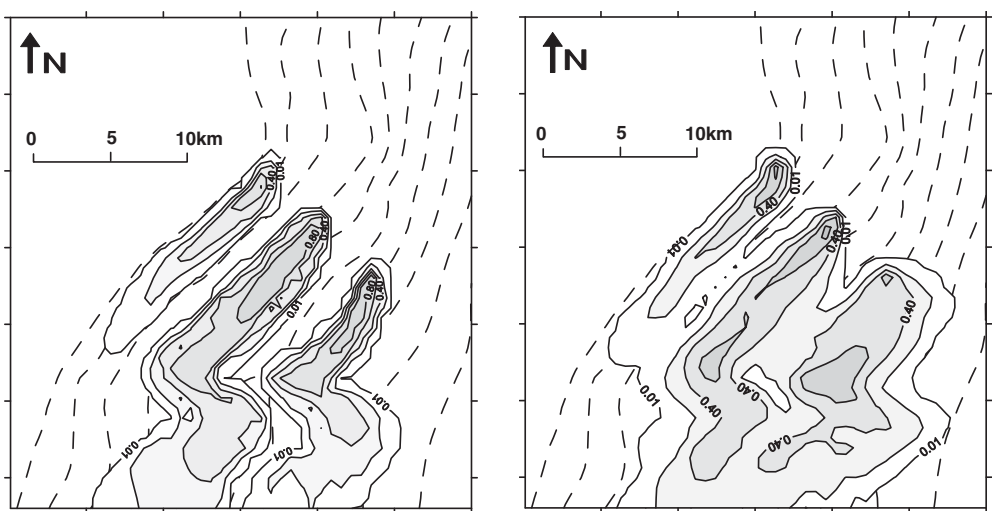

Figure 12. Contour of contaminated probability for continue source under the action of pure waves (a), combined action of waves and tide currents (b). Incident wave height is 2.9 m, period is 7.6 s (24 h).

5. CONCLUSIONS

A numerical model for simulating pollutant transport on the action of waves in the near-shore zone with shallow water is presented in this study, which includes a wave propagation model, a wave-breaking model, a wave-induced current model and a pollutant convection–dispersion model.

The wave propagation model is based on the high-order approximation of mild-slope equation, which can be used to simulate the wave refraction, diffraction and breaking in a large area of near-shore zone, combined with a multi-breaking model. The wave-induced current model is established using the concept of the radiation stress, and the roller contribution to wave breaking is also included in the long-shore momentum balance.

The numerical model is validated by experimental results, which prove that the numerical model is suitable to simulate the wave-induced near-shore current and pollutant transport, especially for a large area of mild-slope beach with shallow water.

The numerical model is also applied in the near-shore zone of Bohai bay. Comparison is made between the distribution of velocities and the pollutant transport under pure waves action and combined action of waves and tide. It is concluded that the pollutant transport will be influenced significantly by the wave action in the near-shore zone with shallow water. The direction of the pollutant transport is approximately parallel to the shoreline and changes with different wave directions. In the design of wastewater outfall locations on a mild-slope beach with shallow water, the position of the outfall should be 10 km away from the shoreline, which is outside of the surf-zone.

ACKNOWLEDGEMENTS

This work was supported by State Key Project of Fundamental Research (973) (2003CB415204) and Key Program of National Natural Science Foundation of China (NSFC) (Grant No. 59839330). The experiments of long-shore current were conducted in the State Key Laboratory of Coastal and Offshore Engineering in Dalian University of Technology.

REFERENCES

1. Holly FM, Usseglio-Pollatera JM. Dispersion simulation in two-dimensional tidal flow. *Journal of Hydyamic Engineering* (ASCE) 1984; **110**(7):905–926.
2. Carreras P, Menendez A. Mathematical modeling of pollutant dispersion. *Ecological Modeling* 1990; **52**: 29–40.
3. Goda Y. A new approach to beach morphology with the focus on suspended sediment transport. *The Proceedings of the First Asian and Pacific Coastal Engineering*, Dalian, 2001; 1–24.
4. Rodriguez A, Sanchez-Arcilla A, Redondo JM, Bahia E, Sierra JP. Pollutant dispersion in the nearshore region: modelling and measurements. *Water Science and Technology* 1995; **32**(9–10):169–178.
5. Tao JH, Han G. Effects of water wave motion on pollutants transport in the near shore area with mild slope beach. *Science in China*, *Series E* 2002; **45**(6):593–605.
6. Madsen PA, Murray R, Sorensen OR. A new form of the Boussinesq equations with improved linear dispersion characteristics. *Coastal Engineering* 1991; **15**:371–388.
7. Berkhoff JCW. Computation of combined refraction diffraction. *Proceedings of the 13th International Coastal Engineering Conference*. ASCE: New York, 1972; 471–490.
8. Radder AC. On the parabolic equation method for water wave propagation. *Journal of Fluid Mechanics* 1979; **95**(1):159–176.
9. Booij N. A note on the accuracy of the mild slope equation. *Coastal Engineering* 1983; **7**:191–203.
10. Kirby JT. Rational approximations in the parabolic equation method for water waves. *Coastal Engineering* 1986; **10**:355–378.

11. Chawla A, Ozkan-Haller HT, Kirby JT. Spectral model for wave transformation and breaking over irregular bathymetry. *Journal of Waterway*, *Port*, *Coastal*, *and Ocean Engineering* (ASCE) 1998; **124**(4):189–198.
12. Longuet-Higgins MS. Longshore currents generated by obliquely incident sea waves, parts 1 and 2. *Journal of Geophysical Research* 1970; **75**:6778–6789 and 6790–6801.
13. Dally WR, Dean RG, Dalrymple RA. Wave height variation across beaches of arbitrary profile. *Journal of Geophysical Research* 1985; **90**(C6):11917–11927.
14. Rattanapitikon K, Shibayama T. Energy dissipation model for regular and irregular breaking waves. *Coastal Engineering* 1998; **40**(4):327–346.
15. Li YC, Yu Y. Experimental study of wave breaking on gentle slope. *Ocean Bulletin* 2000; **19**(1):10–18 (in Chinese).
16. Reniers AJHM, Battjes JA. A laboratory study of longshore currents over barred and non-barred beaches. *Coastal Engineering* 1997; **30**:1–22.
17. Dally WR, Osiecki DA. The role of rollers in surf zone currents. *24th International Conference on Coastal Engineering*, Kobe, 1994; 1895–1905.
18. Osiecki DA, Dally WR. The influence of rollers on longshore currents. *Coastal Engineering* 1996; 3419–3430.
19. Larson M, Kraus NC. Numerical model of longshore currents for bar and trough beaches. *Journal of Waterway*, *Port*, *Coastal and Ocean Engineering* (ASCE) 1991; **117**(4):326–347.
20. Elder JW. The dispersion of marked fluid in turbulent shear flow. *Journal of Fluid Mechanics* 1959; **5**(4): 544–560.
21. Chen Y, Falconer RA. Modified forms of the third-order convection, second-order diffusion equation. *Advances in Water Resources* 1994; **17**:147–170.
22. Sankaranarayanan S, Shankar NJ, Cheong HF. Three-dimensional finite difference model for transport of conservative pollutants. *Ocean Engineering* 1998; **25**(6):425–442.
23. Sun T, Han G, Tao JH. Numerical study of wave-induced long-shore currents and experimental verification. *Journal of Hydraulic Engineering* 2002; **11**:1–9 (in Chinese).
24. Wen S, Yu ZW. *Theories and Calculation Principle for Ocean Waves*. Science Press: Beijing, 1984 (in Chinese).
25. Lin B, Falconer RA. Three-dimensional layer-integrated modelling of estuarine flows with flooding and drying. *Estuarine*, *Coastal and Shelf Science* 1997; **44**(6):737–751.
26. Davies AG, Soulsby RL, King HL. A numerical model of the combined wave and current bottom boundary layer. *Journal of Geophysical Research* 1988; **93**(C1):491–508.
27. Kirby JT. Higher-order approximations in the parabolic equation for water waves. *Journal of Geophysical Research* 1986; **91**(C1):933–952.
28. Soulsdy RL, Hamm L, Klopman G *et al.* Wave-current interaction within and outside the bottom boundary layer. *Coastal Engineering* 1993; **21**:41–69.
29. Sun T, Tao JH. Numerical modeling and experimental verification of pollutant transport under waves in the nearshore zone. *Acta Oceanologica Sinica* 2003; **25**(3):104–112 (in Chinese).

